Heat Transfer and Flow Characteristics of Turbulent Impinging Axisymmetric Air Jet on Corrugated/Ribbed Surfaces

انتقال الحرارة وخصائص الانسياب لنفث هوائي حر دائري مضطرب يرتطم بأسطح متعرجة/ذات زوائد

Gamal H. Moustafa
gamalahemd@Yhoo.com
Dept. of Mech. Power Eng., Faculty of Eng., Port Said University, Port Said, Egypt

يقدم البحث دراسة عملية ونظرية لسريان نفث هوائي صادر من بوق متقارب قطر مخرجه 10 مم يصطدم بجدار ساخن متعرج أو ذي زوائد (بروز) بمساحة مقطع مثلثة أو مستطيلة وارتفاعات مختلفة يوضح بعض من التطبيقات العملية الإليكترونية وضع عموديا في اتجاه سريان من هواء جاف مضغوط بسرعات مختلفة عند مخرج البوق يعطي رقم رينولدز بين 3.4×10^{3} – 1.3×10^{5} 0 وأخذ في الاعتبار تأثير رقم الرينولدز والمسافة البينية بين مخرج البوق وسطح الاصطدام وشكل سطح الاصطدام وارتفاع الزوائد (البروز) والمسافة البينية بين الزوائد وتم قياس توزيع الضغط ومعامل انتقال الحرارة على سطح الاصطدام مع تغيير المسافة البينية بين مخرج البوق وجدار الاصطدام وعولجت الدراسة النظرية بمساعدة معادلات (Navier-Stokes with k-e model) وطبقت طريقة (Finite volume) وقورنت النتائج بتلك في حالة وجود جدار مستوي وبينت الدراسة أن هناك فروق واضحة ومؤثرة بين شكل وتكوين مراحل تطور النفث عند اصطدامه بالجدار المتعرج / ذي الزوائد مقارنة بالجدار المستوي واتضح من الدارسة أن شكل وتكوين النفث بعد الاصطدام يعتمد على عدة عوامل منها : المسافة بين مخرج البوق و سطح الاصطدام ، والسرعة الابتدائية للنفث وكذلك شكل وتكوين سطح الاصطدام والشكل الهندسي للزوائد0 وأعطت الدراسة النظرية صورة واضحة المعالم عن تطور النفث بعد عملية الاصطدام وتأثير شكل سطح الاصطدام على البناء الهيكلي للنفث وكذلك عملية انتقال الحرارة وكان هناك توافق بين النتائج العملية والنظرية (وبينت الدراسة أن عملية تعرج السطح أو وجود الزوائد المصاحب أدت تكسير الطبقة الرقائقية المصاحبة للسريان التي أدت إلى زيادة معامل اضطراب النفث المتولد والمتقدم على الجدار وتكون الدومات مع زيادة نسبة الخلط وجلب كمية أكبر من الوسط المحيط مما رفع معامل انتقال الحرارة عن مثيلتها للسطح المستوي بنسبة تتراوح 19 – 61 % معتمدة اعتماداً كلية على عوامل التشغيل المختلفة المصاحبة للسريان وسطح الاصطدام.

Abstract:
The aerodynamic study of circular normal turbulent jet impinging on a corrugated/ribbed wall is carried out from measurement and numerical analyses of flow and heat transfer fields. The distributions of wall pressure and heat transfer coefficient along the impingement surface are measured at different flow and geometry conditions. Numerical simulations are performed to study momentum and heat transfer characteristics through solutions of Navier-Stokes and energy equations with a turbulence k-e model. The effects of initial flow Reynolds number ($Re=3.4\times10^{3}$:1.3×10^{5}), impact surface geometry (corrugated/ribbed) and surface spacing to nozzle ratio (H/d=2:20) have been analyzed. The results are compared with those of a smooth plate. The obtained results are used to help of understanding the process of the jet impingement on corrugated/ribbed surfaces and its effect on the local heat transfer coefficient between the impinging jet and the complicated surface configuration. This jet impingement results in complicated flow structure in the region confined between the nozzle and target surface. The jet impacts the wall, separates into two parts; each part rolls up along the wall; meets the entrainment and ring vortices are generated. The complex behavior is caused by the generated shear layer, the secondary and recirculating flow created in the entry region over the corrugated target plate or between ribs. This is because the ribs/corrugations break the laminar sub-layer and create local wall turbulence due to flow separation and reattachment behind/inside the ribs/corrugations, and the secondary flow induced by ribs/corrugations, thus greatly enhancing the mixing process, delayed wall separation and improved performance. Experimental data have confirmed the relative corrugation/ribs effects and show different behavior of the wall jet. The spacing between the nozzle and surface strongly influences the flow dynamics. Computational results clearly indicate the structure of the jet impinging corrugated/ribbed surfaces and the effect of spacing between nozzle and target plate. It is observed that the heat transfer coefficient between the impinging jet and the target plate is sensitive to the surface configuration. The increase in the heat transfer coefficient up to 61% depending on the target plate geometry, plate spacing to nozzle ratio and the initial flow Reynolds number is observed. An agreement between measured and numerical results is found.

Keywords: Jet impingement, corrugated/ribbed surface, Navier Stokes, K- ε model, heat transfer, Nusselt number

Accepted August 7, 2011.

Introduction

Impinging jets are commonly used to enhance heat transfer in many modern engineering applications. Therefore, in the last 10 years, there has been much research effort directed at understanding the flow and heat transfer from impinging jet flows. This is because jet impingement systems provide an effective means for the enhancement of convective processes due to the high heat and mass transfer rates that can be achieved. Also, they can remove large amounts of heat over a small area consequently producing high local heat transfer, Beitelmal et al. (2000). The fact is that the high heat transfer rates generated by turbulent impinging jet flows is presented in modern design technologies used by industrial and engineering applications such as the diverse applications, which include the drying of paper, glass manufacturing, material processing, ceramics, gas turbine cascades, heat exchanger, and miniature surfaces like electronic chips. According to the applications, the conditions of impact differ and are defined by many geometrical or dynamic parameters. The main variables for jet impingement heat transfer are the nozzle geometry, the impingement surface configuration, the angle of impingement, the jet Reynolds number, Prandtl number, target plate inclination, roughness of the target plate, curvature of target plate, height of the nozzle above the impingement surface and the turbulence intensity at the nozzle exit, Son, et al. (2001), Wu et al. (2001), Maurel and Solliec (2001), and Taslim et al. (2001). Knowing the effects of these parameters on the heat transfer is necessary for good system development and high efficiency, Chung, et al. (2002). Although many research concentrated on the above knowing parameters, certain gaps remain concerning the configuration of the impinged target plate. Indeed, the majority of the pervious studies relate to a single (or multi) jet impinging on a plane wall. The surface roughness (surface attachment, ribs or grooves) of most mentioned industrial applications can play a significant role in the heat transfer, and thus should not be neglected. In electronic chip cooling, jet impingement is of interest and the high heat transfer rates generated close to the impingement region need to analyze. Ekkad and Kontrovitz (2002) studied the effect of the dimpled surface on the heat transfer between array of circular jets and the flat plate. They reported the reduction in the heat transfer coefficient for the dimpled surface as compared to the smooth surface.

The flow field created by impinging jets is quite complex varying from a stagnation type flow to a wall jet type of flow with considerable curvature of streamlines. If the flow field is confined between an impinging jet and a confinement wall (especially the roughened walls) then recirculation regions may be present as well. Gao et al. (2003) studied the effect of a passive control in the form of triangular taps put at the nozzle exit on the heat transfer rate. Lee et al. (2004) indicated the effect of nozzle exit diameter on the flow field and heat transfer. They reported that the local Nusselt number in the stagnation point region increases with increasing the nozzle diameter. This is attributed to the increase in the jet momentum and turbulence intensity, which in turn results in the heat transfer augmentation at the stagnation point. Zukerman and Lior (2005) studied different numerical modeling and reported correlations for stagnation point and average heat transfer. Beitelmal et al. (2006) analyzed two-dimensional impinging jets and correlated the heat transfers in the stagnation point, stagnation region and wall jet region. Hoffiman et al. (2007) studied the effect of nozzle to plate distance and flow Reynolds number on the flow structure and heat transfer from a single round jet impinging perpendicularly on a flat plate. Comprehensive reviews of heat transfer to impinging jets have been conducted by Varun et al. (2007) and Weigand and Spring (2009) for a wide range of effected parameters. The increase of the distance between the jet and the surface leads to decreasing the local heat transfer significantly, so the remedy is adopting a multiple impinging jets or using rib roughened walls. The effects of important parameters (rib height and pitch) on the heat transfer and pressure drop are needed to understand.

The current research is concerned with the analyses of flow features and heat transfer to impinging air jets over a range of test parameters. These include the initial flow Reynolds number, Re, (from 3.4×10^3 to 1.3×10^5), the intermediate spacing ratio, the impact surface to nozzle exit, H/d, (from 2 to 20), heat flux and target surface configuration, smooth and roughened (ribbed) /corrugated plates. Such a geometry resembles that an electronic component. The mean time average pressure, velocity and temperature distributions up to 12 nozzle exit diameters from the geometric centre of the jet have been reported.

Experimental set up and procedure

The schematic diagram of the experimental set up is shown in Fig.1a. A blow down air supply system has been used to produce the air jet. Compressed air is discharged from two air compressors (1) to an air filter and air dryers, and then to a large storage tank of 8.3 m^3, (2). The maximum pressure in the storage air tank is automatically controlled to approximately 8 bars. The compressed dry air is restored in a settling chamber, (7), (1.75 m long and 0.8 m diameter) after passed through the gate (4) and pressure regulator (5) valves which control the mass flow rate of the air flow. Two mesh wire screens are fixed in the settling chamber to reduce the air disturbances and keep a uniform flow at the nozzle exit. A circular convergent nozzle (15) is made of Aluminum and has dimensions: the length is 35mm, the inlet diameter is 30 mm, and the exit diameter is 10mm. The nozzle is attached to the settling chamber, which is kept parallel to the ground floor. The air is accelerated through the nozzle and released into the ambient atmosphere in the form of a free jet, (10). The air jet is allowed to impinge normally the smooth or corrugated/ribbed plates (11), Fig.1.a. The model configurations are given in Fig.1.b.

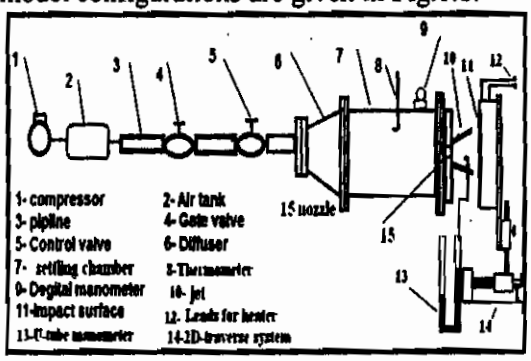

Fig.1a. Schematic diagram of the experimental set up

The target plate has length of 400 mm and width of 400 mm and is instrumented with a 1000mm serpentine Nickel-chromium coil. The heated plate consists of two main layers. The top surface is a 1 mm thick iron plate. A Ceramic plate is fixed to the underside of the iron plate to carry the serpentine heated coil. It has a power rating of 1500 W/m^2 and a voltage rating of 220 V. The voltage is varied using a variable resistance that controls the heat supplied to the upper plate. A two dimensional corrugated and ribbed plates are tested to make understanding the effect of the corrugation and attachment ribs on the heat transfer. The plate assembly is such that it approximates a uniform wall temperature boundary condition, operating typically at a range of surface temperature from 27 °C to 57 °C, in steps of 10 °C. The plate is clamped on a carriage in an arrangement that allows the distance between the nozzle exit and the target plate in the y-direction to be varied; the range is from 2 to 20 nozzle diameters.

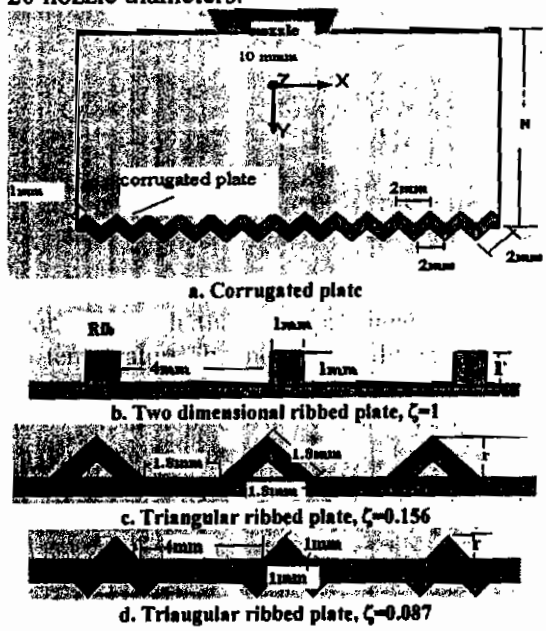

Fig.1b. Schematic diagram of target plates

Measurements of the wall pressure, (p_w) have been done at different values of the stagnation pressure (p_o), in which the corresponding Reynolds number based on the nozzle exit diameter is varied from 3.4×10^3 to 1.3×10^5. The pressure in the settling chamber (p_o), is recorded by a digital manometer (9). The wall pressure (p_w), has been measured through tabs of 0.5 mm inner diameter; made along the surfaces at equal distances starting from the stagnation point. A U-tube water manometer (13) is used to read the wall pressure. The ambient atmospheric pressure (p_a) is measured using a barometer. The temperature in the settling chamber (T_o), is recorded by a digital thermometer (8). Six calibrated Copper-Constantan T-type thermocouples of 0.2 mm outer diameter are distributed over the impingement region to measure the temperature on the target plate. The thermocouples are connected to a digital millivoltmeter. A three dimensional traversing mechanism (14) has a pitch of 1 mm in all directions has been used to change the distance between nozzle and plates, H. The nearest walls have been kept sufficiently far from the tunnel to exclude their effects. The local convective heat transfer coefficient has been calculated from

$$h = \frac{q_v}{T_w - T_f}$$

where q_v is the total heat flux imposed through the electrical resistance and is given by, Lee and Lee (2000)

$$q_v = \frac{IV}{A}$$

The conduction and radiation heat fluxes are considered negligible. The local surface temperature is converted to the local Nusselt number defined as

$$N_u = \frac{hd}{k_f}$$

To perform the experiments, the following procedure is applied. First, the air compressor is turned on and control valves are opened. The pressure and temperature in settling chamber are recorded. The air jet is allowed to impinge the target plate which is located normally with the jet axis by the traverse system. Care is taken into account to find out the jet centerline by a set of pre-experiments. Then, the readings of wall static pressure are recorded. After steady state conditions are reached, the wall and ambient temperatures are recorded.

Uncertainty Estimates

The uncertainty in the measurement is found to be as follows:

* Axial velocity,	u : ± 7%
* Reynolds number	Re: ± 3.2%
* Wall pressure,	p_w: ± 2%
* Tap position,	x/d : ± 3.3%
* Intermediate distance	H/d: ± 3.5%
* Stagnation temperature	T_o ± 2.5%
* Jet air temperature	T_f ± 1.0%
* Wall temperature	T_w ± 0.7%

Numerical model Description

The computational domain is illustrated in Fig. 1b. The turbulent Navier-Stockes and energy equations are solved numerically along with the continuity equation to simulate the flow and thermal fields and compared with experimental data. A mathematical model in three rectangular Cartesian coordinate directions for steady, incompressible flow and constant properties has been applied. The Reynolds average equations in tensor form can be written as

$$\frac{\partial}{\partial x_i}(\rho U_i) = 0 \qquad (1)$$

$$\frac{\partial U_i U_j}{\partial x_j} = \frac{-\partial p}{\partial x_i} + \frac{\partial}{\partial x_j}\left(\mu \frac{\partial U_i}{\partial x_j} - \overline{\rho u_i' u_j'}\right) \qquad (2)$$

$$\frac{\partial U_i T_j}{\partial x_j} = \frac{\partial}{\partial x_j}\left(\mu \frac{\partial T_i}{\mathrm{Pr}\,\partial x_j} - \overline{\rho u_i' T_j'}\right) \qquad (3)$$

The term $\overline{\rho u_i' u_j'}$ represents the Reynolds turbulent stresses and the term $\overline{\rho u_i' T_j'}$ represents the turbulent heat fluxes. The standard k-ε model is the chose since this model has the ability to handle complex high Reynolds number flows in much less time than other turbulent models. This model solves two transport equations one for the turbulent kinetic energy, κ, and the other for the dissipation rate of the turbulent kinetic energy, ε, as shown below:

$$\frac{\partial \rho \kappa U_j}{\partial x_j} = \frac{\partial}{\partial x_j}\left[\left(\mu + \frac{\mu_t}{\sigma_k}\right)\frac{\partial \kappa}{\partial x_j}\right] + \rho(G_b - \varepsilon) \qquad (4)$$

$$\frac{\partial \rho \varepsilon U_j}{\partial x_j} = \frac{\partial}{\partial x_j}\left[\left(\mu + \frac{\mu_t}{\sigma_\varepsilon}\right)\frac{\partial \varepsilon}{\partial x_j}\right] + \rho \frac{\varepsilon}{\kappa}(C_{1\varepsilon} G_b - C_{2\varepsilon}\varepsilon) \qquad (5)$$

where the shear production term, (G_b) is defined as

$$G_b = \mu_t\left(\frac{\partial u_i}{\partial x_j} + \frac{\partial u_j}{\partial x_i}\right)\frac{\partial u_i}{\partial x_j} \qquad (6)$$

the turbulent viscosity, μ_t is given by

$\mu_t = \rho C_\mu \kappa^2 / \varepsilon$.

The model coefficients σ_k, σ_ε, c_1, c_2, and c_μ are 1.0, 1.3, 1.44, 1.92, and 0.09 respectively. The initial values of turbulent kinetic energy and turbulence dissipation are, Patankar, (1970)

$$\kappa_{in} = 1.5 I_u^2 U_o^2, \qquad \kappa_j = 1.5 I_u^2 U_j^2, \qquad I_u = 2\%$$

$$\varepsilon_{in} = \kappa_{in}^{1.5} / \lambda d, \qquad \varepsilon_j = \kappa_j^{1.5} / \lambda d, \qquad \lambda = 0.005$$

where the turbulent kinetic energy, κ_j, and the dissipation rate of the turbulent kinetic energy, ε_j are estimated at the local value of the jet velocity U_j, Kadem et al, (2007).

The numerical computations were performed on non-uniform staggered grid system. A finite volume method described by the following formula was adopted to integrate the considered governing equations (1) to (5).

$$\int_{cv}(\rho \phi u)dv = \int_{cv} div(\Gamma\, grad\phi)dv + \int_{cv} S_\phi dv$$

where ϕ , Γ , S_ϕ are respectively, the transportable quantity, the diffusion term and the source term indicated by governing equations, Imiñe, et al (2005). This gives a system of discretization equations which means that the system of elliptic partial differential equations is transformed into a system of algebraic equations. Then the solution of these transformed equations is performed by implicit line by line Guass elimination scheme. An

elliptic finite volume computer code is used to attain the results of the numerical procedure through using pressure-velocity coupling (SIMPLE algorithm), Patankar (1970). Relaxation factors are used to ensure the solution convergence. The relaxation factors for velocity, pressure and turbulence quantities are 0.5, 1, and 0.7 respectively. Care is taken into account in which the results shown here are sensibly free of grid related numerical errors.

Results and Discussions

The flow field

There has not been a lot of work done on impinging flows in geometries other than smooth plates. In this section, results from a jet impinging normally on ribbed/corrugated surfaces are presented. The impinged surface is heated and a heat transfer has been carried between the jet fluid and the heated surface. The features of the flow field are characterized and sample of data are presented.

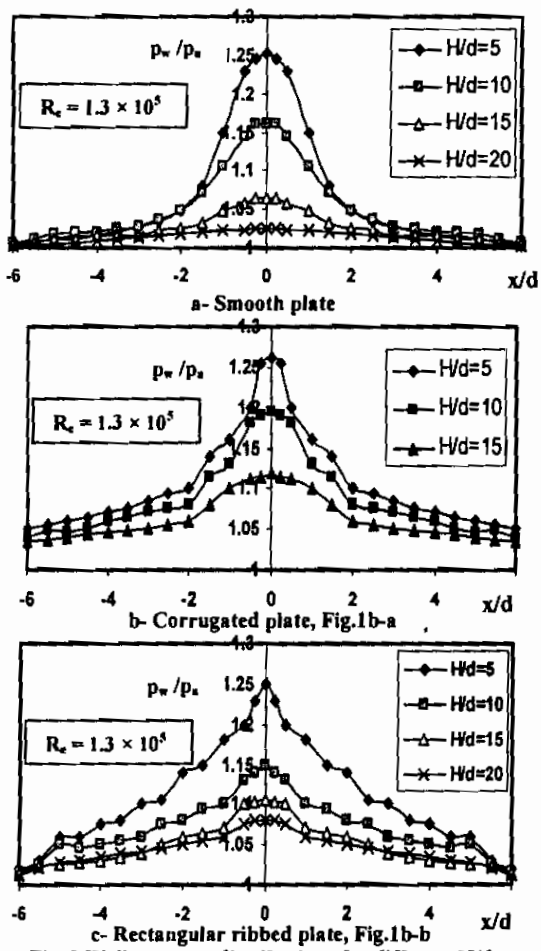

Fig. 3 Wall pressure distributions for different H/d

In Fig.3, the normalized wall pressure distributions (p_w/p_a) for the jet impinging smooth, ribbed and corrugated plates are given for comparison. The Reynolds number is 1.3×10^5 and the distance between the nozzle and plate (H/d) is ranged from 5 to 20. Near the nozzle exit, the jet behaves as a free jet. Experimental results on a jet impinging a smooth plate show a top-hat profile in the region just near the nozzle exit and the maximum pressure is shown along the jet axis. Its value is a function of the intermediate distance between the nozzle and plate. It decreases with increasing the distance between the jet and plate. This is due to the ambient entrainment which increases the spreading and decay of the jet. The pressure decay is almost smooth for the smooth plate while for the corrugated/ribbed plate the profile behaves a steeper dip. This is due to the existence of separated, recirculated and reattached areas appeared on the impinging plate due to the corrugation or attached ribs. As the jet approaches the plate the streamlines turn away from the axis line and the wall jet develops. The pressure decreases as the jet progress along the surface from the symmetry line. At the far distance from the stagnation point, the surface pressure equals the ambient pressure (p_a) and becomes almost constant along the surface; due to the mixing with the ambient. The steadiness of the pressure field is dependent on the geometry of the impinging surface.

The data of the velocity field from the numerical model are represented for various configurations of the target plate for the Reynolds number of 3.5×10^3 and spacing distance, H/d=12. Hence, the typical velocity distributions in the region between the nozzle exit plane and the target plate show an interesting behavior and are given in Fig.4 It is seen that, in the potential core region, i.e. at the section $y/d \leq 2$, the 'top-hat' profiles are almost identical for all cases and similar to that of a free jet, Kadem, et al (2007). As the jet approaches the target plate, an interaction occurs and other peaks are seen at different location from the stagnation point. This is due to the generation of flow vortices generated over corrugated and ribbed surfaces, which stretch and grow gradually downstream through rolling-up process. The growing of flow vortices is affected by the target plate configuration, Gabour and Lienhard (1994) and Narumanchi et al. (2006).

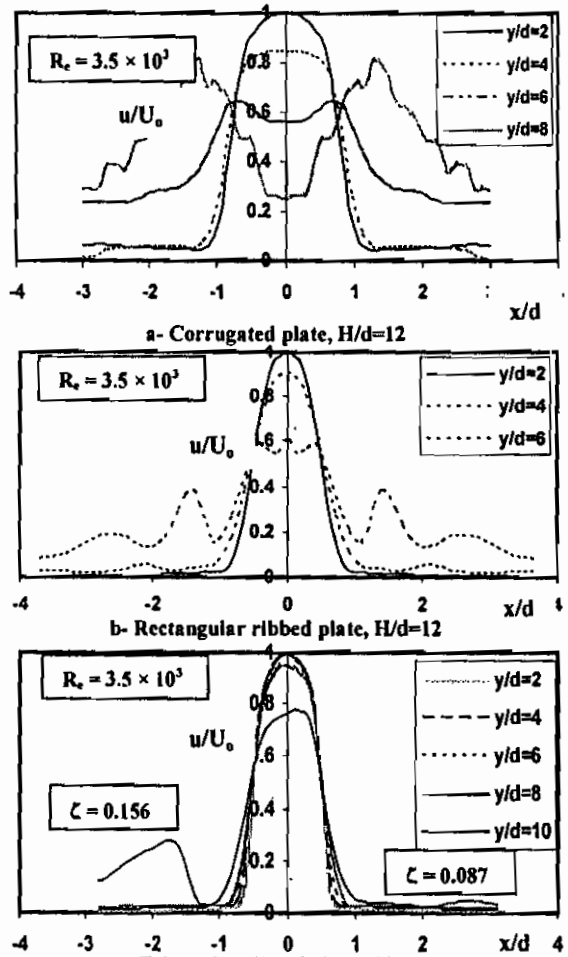

Fig. 4 Velocity field in region between nozzle and target plate

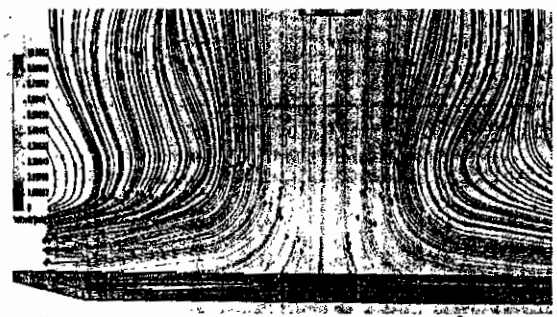

Fig. 5 Flow field on a smooth plate, Re=6.7× 10^3, H/d=5

Calculations have been done to complement the experimental data to provide further insight into the structure of the corrugated/ribbed surfaces. The computed isolines, contours and trajectories of the velocity field from the present simulation are given in Fig. 5, for the jet impinges the smooth plate. The initial Reynolds number, R_e=6.7×10^3 and the spacing distance, H/d=5. These snaps increase understanding of the general structure, flow field features, streamwisw trajectory behaviour, and scaling properties of the round jet impinging on the smooth plate. It is seen that the calculation provides qualitative agreement with the experimental data. Near the nozzle exit, the free jet is formed and the potential core is depicted. Far from the nozzle, the interaction with the target plate occurs and the ambient entrainment is illustrated by the curvature of the velocity lines. The streamwise velocity lines turn smoothly along the plate, out from the symmetry line in which the wall jet is developed. Along the impingement plate, the wall jet progress, develops and diverges in the far region from the symmetry line.

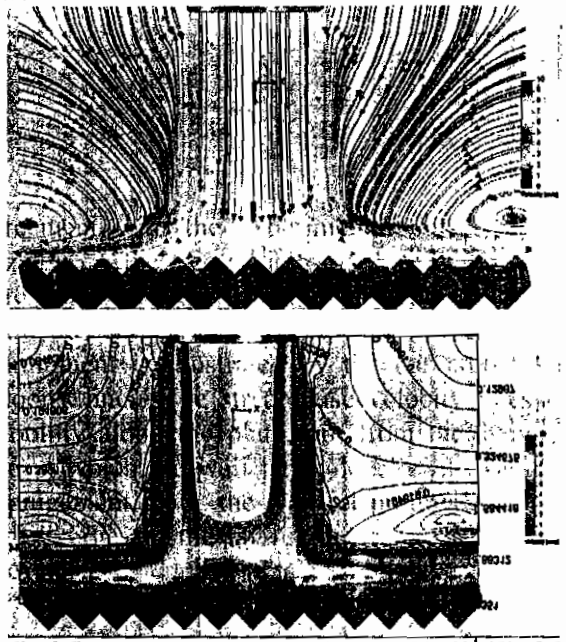

Fig. 6 Flow field on a corrugated plate, Re=7.1× 10^4, H/d=2.5

The numerical solution has also reproduced the expected physical features of the jet impinging corrugated plates, Fig.6. The developed region near the nozzle exit, the core region, interaction zone, reflection, and entrainment are clearly shown. The fluid emanating from the jet decelerates in the axial direction at the impinged surface. The flow then turns sharply and forms a wall jet along the upper surface of the plate. For the case of the smooth plate, Fig.5, the wall jet progress smoothly with almost constant pressure. However for the case of the corrugated plate, Fig.6, the jet approaching the plate will at some intermediate distance begin to feel the presence of the plate. The flow separatcs and reattaches the v-shaped channel (corrugated structure). Secondary flows, wall eddies and different bubbles of different lengths are formed inside each channel. This is due to the strong influence of the outer region of the impinging jet and the axisymmetric nature of the flow. The ambient fluid outside the jet is entrained into the core with a developing shear layer separating the core and the ambient. This entrainment is illustrated by the curvature of the velocity lines outside the jet

towards the symmetry axis and leads to a small recirculation zone in the vicinity of the exit jet-wall. This feature and the presence of a secondary recirculation near the bottom of the v-shaped indicate sufficient flow vortices around the stagnation point. The convected wall eddies induced from the interaction process stretch and grow downstream. This creates a large scale toroidal vortices and recirculation region that has a significant effect on the wall heat transfer. Far from the symmetry line, the flow progress parallel to the surface in which the wall jet is redeveloped. Due to the growing process of the wall vortices, the ambient entrainment shows generation of flow eddies, which affect the development of the wall jet. Thus, the nature of the wall jet is different from that of the smooth plate, Fig.5.

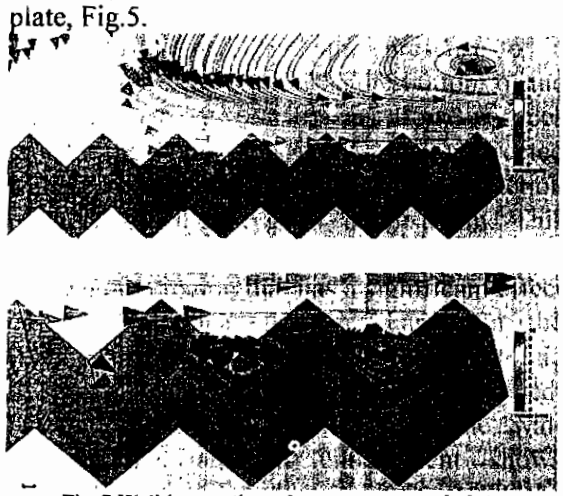

Fig. 7 Wall jet, vortices along a corrugated plate, Re=7.1× 10^4 , H/d=2.5

Making a focus on the flow characteristics along the corrugated plate has done to understand the fluid flow and heat transfer of the jet impinging a corrugated plate especially the generated wall jet, Fig.7. An interesting behavior is depicted; the numerical model successes to provide the best view for the flow field. The isolines of mean averaged velocity turn away from the jet axis, the wall jet progress along the surface, the flow separates from the top of corrugated channels, flow recirculation and large scale torodial vortices and eddies are visible. Many bubbles are formed in the v-shaped channel along the corrugated plate. Each one has different length from the other. This length develops, stretches and grows as the flow progress along the plate. The large scale length is shown at the end of plate with increasing the amount of surrounding entrainment resulting a recirculating zone and counter-rotating vortex pairs. This leads to an enhancement of the mixing process, which means that the centrifugal force increases as the flow progress along the surface, so that an increase in the recirculation force occurs which enhances the wall heat transfer.

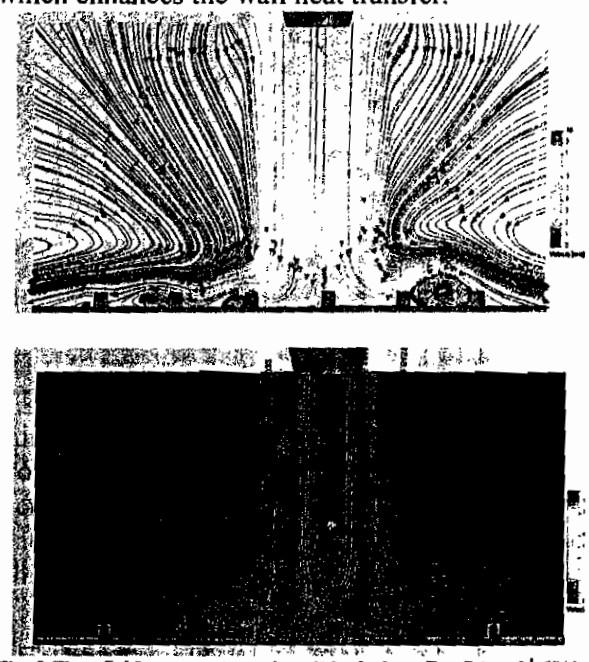

Fig. 8 Flow field on a rectangular ribbed plate, Re=7.1× 10^4, H/d=5

The vertical near-field flow structure of the jet impinging on a two dimensional rectangular ribbed surface is numerically visualized and typical results are shown in Fig.8. The flow is parallel to the jet axis at the nozzle exit, develops into a free jet. Ambient fluid is entrained into the core of the jet prior to impingement. This entrainment is shown by the curvature of the ambient velocity lines towards the symmetry axis. The flow decelerates as it impinges on the top of the ribs. At the corners of each rib, the flow separates, reattaches downstream on the base plate between each two ribs. Different recirculation zones are formed at the two sides of each rib and many vortices are formed. As the jet progresses along the plate, flow vortices are stretched and their sizes grow gradually through rolling-up process. The toroidal vortices grow over the impingement plate periodically and a large scale one is shown at a distance of x/d = 1.0. The behavior of the wall jet is affected by the generation of such wall flow vortices. After the impingement, the large-scale vortices stretch and grow in the x-direction along the wall surface and interact with the impingement plate. The convected wall eddies induced from interaction between the large-scale toroidal vortices and the impingement surface can be clearly seen in the region ranged as $1.0 \leq x/d \leq 2.0$. The wall eddies are stretched and diverged in the downstream from the symmetry line in some pulsating patterns. With going further on the plate,

the toroidal vortices and the induced wall eddies are abruptly merged with the surrounding entrainment. This leads to change the structure and nature of the wall jet; transformed into a turbulent wall jet.

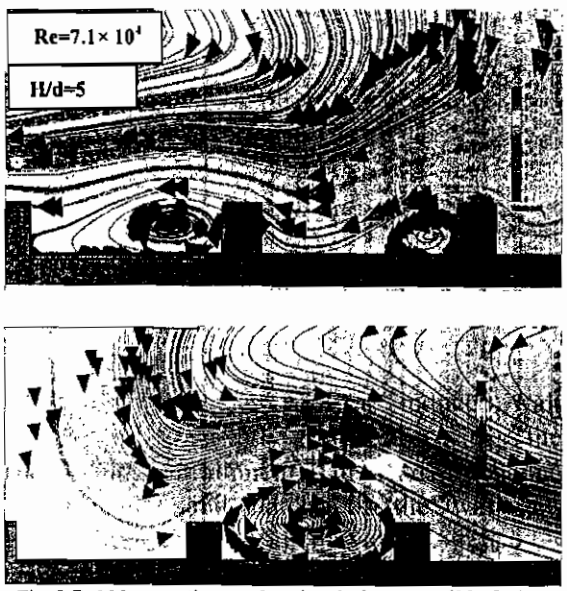

Fig. 9 Bubbles, vortices and recirculation on a ribbed plate

The complex features of the turbulent wall jet induced from the interaction of the jet and ribbed target plate include entrainment, stagnation, streamline curvature and a change in the flow direction due to the ribs and wall eddies. As the wall jet progresses downstream, the structure of recirculation zone is changed by the ribs with increasing its length. At the far region, the wall vortices stretch, grow and fill the entire region between the two ribs, Fig.9. At this instant, the wall jet changes its direction and the intermediate spacing between the velocity lines decreases. This results in a very complex flow structure with several flow-related phenomena, such as stagnation points, separations, recirculation, vortices, bubble generation and curvature effects, which have influences on the heat transfer rate, Fig.4.

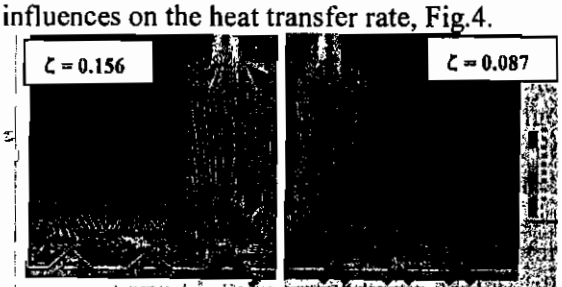

Fig. 10 Structure of flow field on a triangular ribbed plate
Re=7.1× 10⁴, H/d=3

The velocity field from the numerical model is illustrated by contour plots of the velocity magnitude in the xy-plane for the jet impinging on a triangular shaped ribbed plate, Fig.10. Two values of the height of the triangular ribs are considered. In the lift snap, the height is 1.56mm, $\zeta = 0.156$ and in the right snap the height is 0.87 mm, $\zeta = 0.087$. The flow field shows a complex behaviour depending on the rib height. There are several flow-related phenomena that can affect the structure of the flow field, the initial flow Reynolds number, the spacing between the nozzle and target plate, the height of ribs and the interior distance between ribs. Three zones can be identified: firstly there is a free jet zone, which is the region that is largely unaffected by the presence of the impingement ribbed surface; this exists beyond approximately 1.5-3.5 diameters from the nozzle exit, depending on the initial flow Reynolds number and spacing between the nozzle exit and target plate. A potential core exists with the free jet region, within which the jet exit velocity is conserved and the turbulence intensity level is relatively low. A shear layer exists between the potential core and the ambient fluid where the turbulence is relatively high and the mean velocity is lower than the jet exit velocity. The shear layer entrains ambient fluid and causes the jet to spread in the direction normal to the jet axis. Beyond the potential core the shear layer has spread to the point where it has penetrated to the centreline of the jet. At this stage, the centreline velocity decreases and the turbulence intensity increases, especially for higher values of the rib height, the lift snap of Fig.11. The snaps also identify a stagnation zone that extends to a location in the x-direction defined by the spread of the jet. The stagnation zone includes the stagnation point where the mean velocity is zero and within this zone the free jet is deflected into the wall jet flow. The surface ribs break the shear sub-layer associated with the wall jet and create local wall turbulence due to the flow separation and reattachment over and behind the ribs, Fig.11. The secondary flow induced by these ribs, creates recirculating and flow vortices, thus greatly enhancing the mixing process and improved the wall heat transfer process.

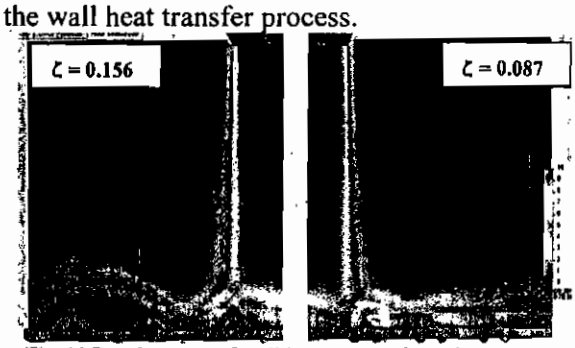

Fig. 11 Development of wall jet along a triangular ribbed plate
Re=7.1× 10⁴, H/d=3

The length scale of flow vortices induced by the interaction between the jet and triangular ribs depends on the surrounding entrainment, height of ribs, the interior distance between ribs and the position from the jet axis, Fig.12. A strong influence of the rib height on the flow dynamics is observed. This effect is similar to that found with the plate has attached rectangular ribs. However, making a focus on the snap, the triangular ribs cause the ring vortices to be spaced less closely together than for the case of rectangular ribs, Fig.13.

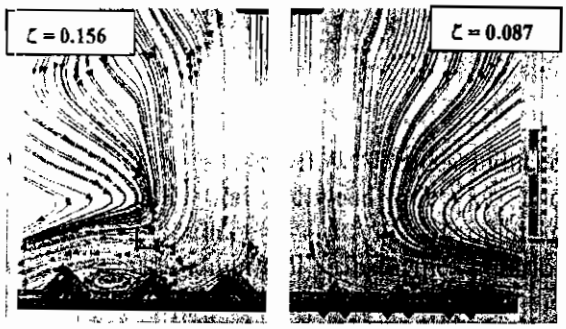

Fig. 12 Effect of rib height on the flow field, Re=7.1× 10^4, H/d=5

Fig. 13 Induced ring vortices along a triangular ribbed plate, Re=7.1× 10^4, H/d=5

The temperature field

Fig.14 shows the variation in the measured Nusselt number in the x-direction along the smooth plate for different Reynolds number and H/d = 4. In general, it is observed that the Nusselt number increases as the flow Reynolds number is increased. The rate of increase is higher at the stagnation point as compared to the other location along the target plate in the x-direction. For an increase in the Reynolds number from 3.5 × 10^3 to 7.1×10^3, the Nusselt number at the stagnation point increases from 53.7 to 86.4 (i.e., 61%) whereas at a location corresponding to x/d=10, the increase in the Nusselt number is from 30.4 to 42.3 (i.e., 39%). This suggests that the stagnation point heat transfer is stronger function of Reynolds number than the wall jet heat transfer. The same results were reported by Kadem et al. (2007) for an axisymmetric turbulent jet impinging on a flat plate.

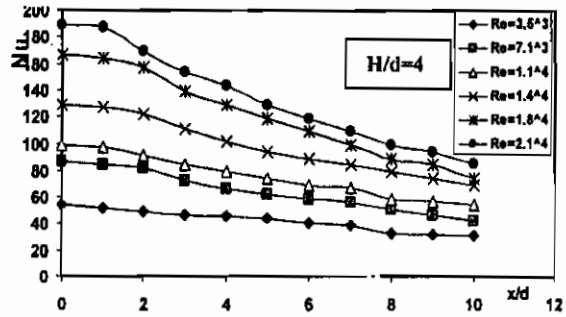

Fig. 14 Effect of Re on temperature distribution along smooth plate

The variation of the calculated stagnation point Nusselt number for the smooth plate with the initial flow Reynolds number is given in Fig.15. The spacing between the nozzle exit plane and target plate, H/d=8. A comparison with the measured data is shown, an agreement is found.

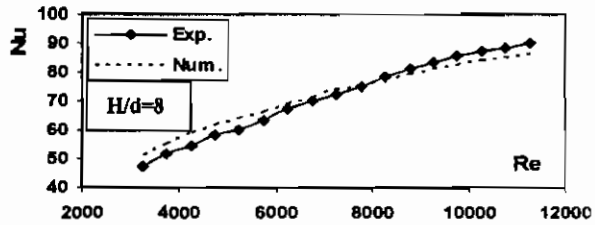

Fig. 15 Numerical and measured Nu vs. Re for a smooth plate

Fig. 16 gives the comparison of the calculated Nusselt number for smooth and corrugated surfaces at a Reynolds number of 1.1×10^4 and nozzle to plate spacing, H/d=6. The solid corrugated line indicates the quantities values of the Nusselt number at the top and base points of the corrugated plate. The mean averaged values are correlated and given by the detach point line. An increase in the Nusselt number can be observed for the corrugated plate as compared to that of the smooth plate. For example, at the stagnation point, the Nusselt number increases from 68 to 90.46 (i.e., 33%) whereas at a location in the x-direction corresponding to x/d=6, the increases in the local Nusselt number is from 26 to 34.97 (i.e., 34.5%). This indicates that there are significant effects of wall vortices and bubbles induced by the wall jet over the corrugated plate on the augmentation of the heat transfer.

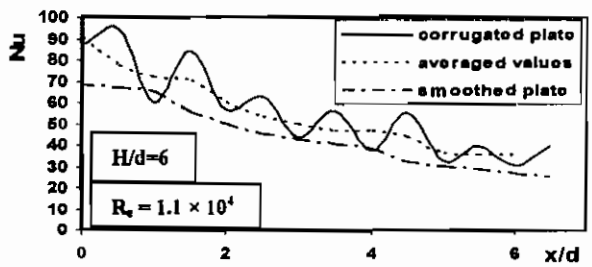

Fig. 16 Variation of Nusselt number along a corrugated plate

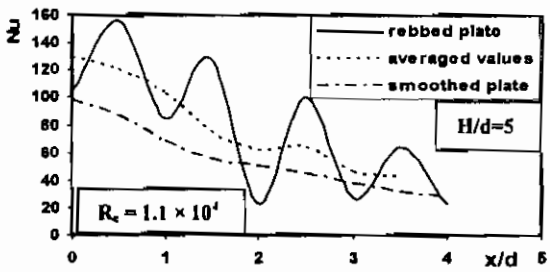

Fig. 17 Variation of Nu along a rectangular ribbed plate

Fig.17 shows the comparison of the Nusselt number for the smooth and rectangular ribbed target plate at a Reynolds number of 1.1×10^4 and nozzle to plate spacing, H/d=5. The solid corrugated line indicates the quantities values of the Nusselt number at the top and middle points on the base between ribs. An increase in the Nusselt number is found as compared to that of the smooth plate. This means that the attached ribs generate wall vortices and recirculation of eddies, which increase the flow mixing as well as the heat transfer. The increase in the Nusselt number ranges between 31.8% and 38.7% depending on the location in the x-direction from the stagnation point.

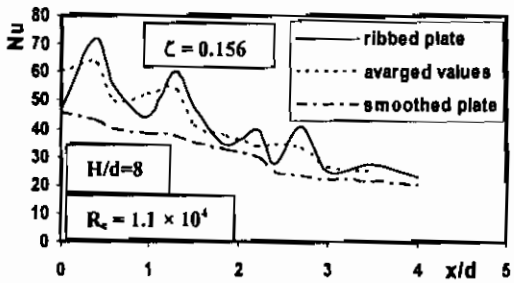

Fig. 18 Variation of Nu for triangular ribbed plate

Fig.18 shows the comparison of the Nusselt number for the smooth and triangular ribbed target plates at a Reynolds number of 1.1×10^4 and nozzle to plate spacing, H/d=8. Also, the same feature of the Nusselt number variation along the target plate as those of the corrugated and rectangular ribbed plate is observed. An increase in the Nusselt number is found as compared to that of smooth plate. The increase in the Nusselt number ranges between 19% and 32% depending on the location in the x-direction from the stagnation point. It can be concluded that there is an overall increase in the heat transfer for the corrugated and ribbed surfaces as compared to that of the smooth surface. But, the increase in the Nusselt number depends on the initial flow Reynolds number, the spacing between the nozzle and surface, the surface configuration and the location from the stagnation point.

Conclusions

The fluid flow and heat transfer characteristics of a turbulent circular air jet impinging normally on a heated corrugate/ribbed target wall are examined using experimental and numerical simulations. The effects of nozzle to target plate spacing, Reynolds number and target plate configuration are considered. The range of Reynolds numbers examined is from 3.4×10^3 to 1.3×10^5. The distance of the target plate from the nozzle exit plane varies between 2 to 20 the nozzle exit diameters. Different data for the pressure distribution, velocity and temperature fields are obtained. The results of experimental and computational studies show that there is a significant enhancement in the local heat transfer. The corrugated and ribbed surfaces produce much flatter velocity profile and higher turbulence intensities as compared to the smooth surface. This is because the ribs/grooves break the laminar sub-layer and create local wall turbulence due to flow separation and reattachment behind/inside the ribs/grooves, and the secondary flow induced by ribs/grooves, thus greatly enhancing the mixing process, delayed separation and improved performance. It is also observed that the heat transfer coefficient is sensitive to the configuration of the target plate. The increase in the Nusselt number from 19 % to 61% depending on the target plate configuration, spacing between the nozzle and plate, the distance from the stagnation point and the initial flow Reynolds number is observed. The numerical solution success to reproduce the flow details which increases the understanding for the method of heat transfer enhancement.

Nomenclature

A: the surface heated area, m^2
d : nozzle exit diameter, m
H: distance between nozzle and surface, m
h: heat transfer coefficient, W/m^2 K
k_f : Thermal conductivity of fluid, W/m K
p : pressure , N/m^2
U_o : mean velocity at nozzle exit, m/sec
u: velocity in axial direction, m/sec
r: rib height, m
Re: Reynolds number ($\rho U_o d / \mu$)
T_f: jet air exit temperature, K
T_w: local wall temperature, K
ε : turbulence dissipation, m^2/sec^3
κ : turbulent Kinetic energy, m^2/sec^2

μ : dynamic viscosity, kg/m sec
ρ : air density, kg/m^3
ζ : rib height/nozzle diameter, r/d

Subscripts
a : Ambient condition
o : Stagnation (settling chamber) condition
w : wall condition

References

[1]-Beitelmal, A.H., Saad, M.A., Patel, C.D., "The Effect of Inclination on the Heat Transfer Between a Flat Surface and an Impinging Two-Dimensional Air Jet", Int. J. Heat Fluid Flow, Vol. 21,2000,156–163.

[2]-Beitelmal A.H., Shah, A.J., and Saad, M.A., "Analysis of an Impinging Two-dimensional Jet", ASME, J. Heat Transfer, Vol. 128, 2006, pp. 307-310.

[3]-Chung, Y.M., Luo, K.H., and Sandham, N.D., "Numerical Study of Momentum and Heat Transfer in Unsteady Impinging Jets", Int. J. Heat Fluid Flow, Vol. 23,2002,592–600.

[4]-Ekkad, S.V., and Kontrovitz, D, "Jet Impingement Heat Transfer on the Dimpled Traget Surface", Int. J. Heat Fluid Flow, Vol. 23, 2002, pp. 22-28.

[5]-Gabour, L.A., and Lienhard V, J.H., "Wall Roughness Effects on Stagnation Point Heat Transfer beneath an Impinging Liquid Jet", Journal of Heat Transfer, ASME, Vol. 116, Feb. 1994, pp. 81-87.

[6]-Gao, N., Sun, H., and Ewing, D., "Heat Transfer to Impinging Round Jets with Triangular tabs", Int. J. Heat Mass Transfer, Vol. 46, 2003, pp. 2557-2569.

[7]-Hofmann, H.M., Kind, M., and Martin, H., "Measurements on Steady State Heat Transfer and Flow Structure and New Correlations for Heat and Mass Transfer in Submerged Impinging Jets", Int. J. Heat Mass Transfer, Vol. 50, 2007, pp. 3957-3965.

[8]-Imine, B., Saber-Bendhina, A., Imine, O. and Gazzah, M.H., "Effect of a Directed Co-flow on a Non-Reactive Turbulent Jet with Variable Density", Heat Transfer, Vol.42, (2005), pp. 39-50

[9]-Kadem, N, Mataoui, A., Salem, A., and Younsi, R., "Numerical Simulation of Heat Transfer in an Axisymmetric Turbulent Jet Impinging on a Flat Plate", AMO-Advanced Modeling and Optimization, Vol. 9, No. 2, 2007, pp.207-217.

[10]-Lee, J., and Lee, S., "The Effect of Nozzle Aspect Ratio on Stagnation Region Heat Transfer Characteristics of Elliptic Impinging Jet", Int. J. of Heat and Mass Transfer, Vol.43, 2000, pp. 555-575.

[11]-Lee, D.H., Song, J., and Myeong Chan Jo., "The Effect of Nozzle Diameter on Impinging Jet Heat Transfer and Fluid Flow", J. Heat Transfer, Vol. 126, 2004, pp. 554-557.

[12]-Maurel, S., and Solliec, C., "A Turbulent Plane Jet Impinging Nearby and Far from a Flat Plate," Exp. in Fluids, Vol. 31, 2001, pp. 687–696.

[13]-Narumanchi, S., Hassani, V., Bharathan, D., and Troshko, A. "Numerical Simulations of Boiling Jet Impingement Cooling in Power Electronics", NREL/CP-540-39401, Dec. 2006.

[14]-Patankar, S.V., "Numerical Heat Transfer and Fluid Flow", McGraw-Hill, New-York, 1970.

[15]-Son, C., Gillespie, D., Ireland, P., and Dailey, G., "Heat Transfer and Flow Characteristics of an Engine Representative Impingement Cooling System", J. of Turbomachinery, Vol. 123,2001, pp. 154–160.

[16]-Taslim, M.E., Pan, Y. and Spring, S.D., "An Experimental Study of Impingement on Roughened Airfoil Leading-Walls with Film Holes," J. of Turbomachinery, Vol. 123, No. 4, 2001,pp. 766-773.

[17]-Varun, R, Saini, R.P., and Singal, S.K., "A review on Roughness Geometry Used in Solar Air Heaters", Solar Energy, Vol. 81, 2007, pp. 1340-1350.

[18]-Weigand, B., and Spring, S., "Multiple Jet Impingement – A Review", Int. Symp. on Heat Transfer in Gas Turbine Systems, 9-14 August 2009, Antalya, Turkey.

[19]-Wu, J., Tang, L., Luke, E.A., and Tong, X., "A Comprehensive Numerical Study of Jet Flow Impingement over Flat Plates at Varied Angles," AIAA–2001–0745, Jan. 2001.

[20]-Zukerman, N. and Lior, N., "Impingement Heat Transfer: Correlations and Numerical Modeling", J. Heat Transfer, Vol. 127, 2005, pp.544-552.